Article

Ultrasensitivity of microtubule severing due to damage repair

Chloe E. Shiff, Jane Kondev, Lishibanya Mohapatra

lxmsps@rit.edu

Highlights

Past experiments show tubulin repairing severing protein-induced damages on microtubules

Theoretical analysis describes severing as a contest between damage spreading and repair

Model predicts a regime where severing probability is sensitive to tubulin concentration

Varying free tubulin dramatically changes steady-state microtubule lengths

Article

Ultrasensitivity of microtubule severing due to damage repair

Chloe E. Shiff,[1] Jane Kondev,[2] and Lishibanya Mohapatra[3,4,*]

SUMMARY

Microtubule-based cytoskeletal structures aid in cell motility, cell polarization, and intracellular transport. These functions require a coordinated effort of regulatory proteins which interact with microtubule cytoskeleton distinctively. *In-vitro* experiments have shown that free tubulin can repair nanoscale damages of microtubules created by severing proteins. Based on this observation, we theoretically analyze microtubule severing as a competition between the processes of damage spreading and tubulin-induced repair. We demonstrate that this model is in quantitative agreement with *in-vitro* experiments and predict the existence of a critical tubulin concentration above which severing becomes rare, fast, and sensitive to concentration of free tubulin. We show that this sensitivity leads to a dramatic increase in the dynamic range of steady-state microtubule lengths when the free tubulin concentration is varied, and microtubule lengths are controlled by severing. Our work demonstrates how synergy between tubulin and microtubule-associated proteins can bring about specific dynamical properties of microtubules.

INTRODUCTION

Cells contain a cytoskeleton that aids in various cellular processes such as maintaining cell polarization, motility, and transport. The cytoskeleton is highly dynamic—it is composed of various structures that are constantly built and dismantled to assist in various functions. For example, the single-cell alga Chlamydomonas uses microtubule-based flagella for motility.[1,2] Microtubule-based fibers in the mitotic spindle shorten for chromosome separation during mitosis and meiosis.[3–5]

Such dynamic changes in cytoskeletal structures require a rapid turnover which involves an exchange of their molecular building blocks (that is freely diffusing in the cytoplasm) with the pool. The time scales associated with turnover of cytoskeleton filaments *in vivo* are quite different from those measured *in vitro*, as a result of regulatory proteins that exist in cells that interact with cytoskeleton proteins. While actin networks within cells are disassembled on the order of seconds, the process takes a few minutes *in vitro*.[6–9] Similarly, the polymerization rate of tubulin *in vivo* is about five to ten-fold higher than *in vitro* at a similar concentration of free tubulin.[10,11] Further, microtubules are known to switch between phases of slow growth and rapid shrinking by a process known as dynamic instability, which has been studied extensively *in vitro*.[10] The rates of switching from shrinking to growth and vice versa (called rates of rescue and catastrophe, respectively) are sensitive to, and are believed to be modulated by several microtubule-associated proteins *in vivo*.[12–16] Turnover rates can also be different at different stages of the cell cycle – for example, microtubule turnover rates measured in *Xenopus* extracts range from 3 min to 20s during interphase and mitosis, respectively.[4] While much is known about the biochemical processes that facilitate the turnover of these structures in isolation from *in vitro* studies, it is still not clear how different cytoskeleton-associated proteins work together to promote filament turnover in cells.

Recently, several studies have addressed this question by combining multiple regulatory proteins with cytoskeletal filaments *in vitro* and have reported novel synergistic effects.[17] Cofilin-induced depolymerization rate of actin filaments increases 200-fold in the presence of cyclase associated protein/Srv-2.[18] Similar studies have been done using microtubules with a recent study finding that collective effects of microtubule-associated proteins like MCAK and XMAP215 can lead to microtubule treadmilling.[19] Here, inspired by recent experiments, we consider the interplay between the free pool of tubulin dimers and microtubule severing proteins, which bind to the sides of microtubules and break them into two.[20]

Free tubulin is known to affect microtubule dynamics by modulating rates of nucleation and polymerization.[14,21–23] Notably, using FRET, it was shown that a local release of tubulin promoted microtubule extensions into lamellipodia, demonstrating a feedback between filament-bound and free tubulin pools.[24] However, there are also reports of free tubulin affecting microtubule disassembly via its interactions with proteins such as kinesin-13,[12,25] kinesin-8[26,27] and severing proteins.[20,28] Here we theoretically describe the effect of free tubulin on microtubule severing via a recently discovered process of tubulin-induced repair of damages to the microtubule lattice by severing proteins.[20]

[1]Institute for Computational and Mathematical Engineering, Stanford University, Stanford, CA 94305, USA
[2]Department of Physics, Brandeis University, Waltham, MA 02454, USA
[3]School of Physics and Astronomy, College of Science, Rochester Institute of Technology, Rochester, NY 14623, USA
[4]Lead contact
*Correspondence: lxmsps@rit.edu

Severing proteins can play a key role in the reorganization of the cytoskeleton by breaking down existing structures and freeing up monomers for use in new structures.[29–31] Recent studies have found that severing proteins can seed new filament growth by releasing filaments from nucleation sites and allowing their transport within the cell.[30] Katanin, fidgetin, and spastin are well characterized examples of severing proteins for microtubule-based structures,[32–35] while cofilin and Srv-2 sever actin-based structures.[28,36–39] Katanin is thought to play two functions in mitosis and meiosis – to amplify the number of microtubules in the spindle and to uncap microtubule plus ends from the kinetochore and enable depolymerizing kinesins to target microtubules.[30] Inhibition of katanin results in abnormally long mitotic spindle length in *Xenopus* extracts.[40] Severing proteins play an important role in neurons as well.[41] It has been proposed that katanin stimulates axon growth by releasing microtubules from centrosomes and severing them into shorter segments that can be transported along longer microtubules down the axon to seed new microtubule growth.[42] Mutations in *Drosophila* spastin reduce dendritic arborization (branching),[43] suggesting that spastin seeds microtubule growth within newly forming regions of the dendrite.

Electron microscopy images of microtubules have revealed the mechanisms by which severing proteins induce a break in the microtubule. One study reported that once severing proteins land on a microtubule, they create nanoscale damages[20] and found that not all of the damage sites proceeded to a severing event, as free tubulin could repair the damage.[20] Additionally, some experimental studies have also reported free tubulin in solution can reduce the amount of severing,[44] delay the severing onset and prolong the severing process.[45] Further, *in-vitro* studies and computational studies have reported that severing proteins promote the regrowth of severed microtubules by enhancing the rate of rescue in microtubules[46,47] and lead to a net increase in microtubule number and mass.[20,28,29,48,49] It is unknown whether severing proteins have the same effect *in vivo* where they interact with other microtubule-associated proteins. Interestingly, incorporation of new tubulin dimers into microtubule lattice has also been reported at defects arising from mechanical stress,[46,47] or damages created by molecular motors.[50,51]

Severing proteins have another remarkable property that we explore in this paper, namely they can control the lengths of cytoskeletal filaments. The probability that a severing protein which is diffusing in solution lands on a filament is proportional to its length.[52] Therefore, the process of severing is a length-dependent disassembly mechanism wherein longer filaments are more likely to be severed. This results in negative feedback of filament length on a growing filament and leads to control of length of cytoskeletal filaments. This property of severing proteins has been explored by a number of theoretical and experimental studies,[28,46–49,53–56] however, how these proteins work with other proteins to control the sizes of filamentous structures *in vivo* is not well understood.

Flagella in *Chlamydomonas*[2,57,58] and *Giardia*,[59,60] and the mitotic spindle[40] are well studied examples of microtubule-based structures that are known to maintain size. Control of the size of these structures can arise by controlling the nucleation, as observed in the context of spindles[61] or the rates of elongation - achieved by modulating either the assembly as proposed in flagella in *Chlamydomonas*[2,62] or the disassembly of these structures.[29,63,64] Recently, disassembly proteins kinesin-13 were shown to control flagella lengths in *Giardia*.[64] Severing proteins, that are the focus of this study, have been shown to modulate microtubule lengths in neurons[42] and alter the size of spindles *in vivo*.[29,40] How severing proteins work in conjunction with other cytoskeletal proteins to control sizes of these structures *in vivo* is an open area of investigation. Here, we consider theoretically the role of severing proteins in controlling the length of microtubules and how their length-control function is altered by tubulin-induced microtubule repair.

Inspired by recent experimental observations,[20,45–47,56] we consider a theoretical model for microtubule severing that incorporates the newly discovered repair process by free tubulin. Using theory and simulations, we show that this model, suggested previously,[20] quantitatively agrees with *in vitro* experiments and makes predictions for new *in vitro* experiments. Significantly, we predict the existence of a critical tubulin concentration above which severing becomes rare but fast. This model also has several implications for the dynamics of microtubules *in vivo* - we show that length control via severing is ultrasensitive to changes in tubulin concentrations, resulting in a dramatically expanded dynamic range of filament lengths. We also report the probability distribution of lengths, the mean length and its coefficient of variation as a function of the model parameters, which can be used to test the model. In summary, our work describes how the concerted action of tubulin and severing proteins produces dynamical properties of microtubules that are not seen when these proteins are studied independently.

RESULTS

Model of microtubule severing with repair

Inspired by recent experiments,[20,44,45] we consider that a microtubule severing event begins when a severing protein lands on a filament, binds to the side, and creates a damage spot (Figure 1A). The fate of the damage created by a severing protein is determined by a competition between the removal and addition of tubulin at the damage site, eventually leading to severing or repair as suggested in ref.[20,31] In our model we do not take into account the geometry of the damage sites, how they are arranged in the two-dimensional lattice of tubulin dimers at the surface of a microtubule. Instead, we consider a coarse-grained model of damage spreading that only keeps track of the size of the damage in terms of the number of tubulin dimers that have been removed. A further simplifying assumption in describing the spreading is that the rates of adding or removing a tubulin dimer, which increase or decrease the size of the damage by one, are constant and do not depend on the size or geometry of the damaged region.

We assume that tubulin dimers ("subunits") are added to the damage site at a rate proportional to the concentration of free tubulin $k_T[T]$ (s^{-1}) and are removed from the damage site at a rate k_r (s^{-1}). If the size of the damage reaches N_D removed tubulins, the filament is severed. On the other hand, if the size reaches zero, then the damage is repaired. In this way, the size of the damage (x, measured in subunits) is modeled as a one-dimensional random walk with absorbing boundaries at $x = 0$ and $x = N_D$ (Figure 1B).

In this model of severing with repair, a damage site can either be repaired or progress to a severing event. Using the classic one-dimensional random walk model to describe the growth of damage size, we find an analytical expression for the probability of severing (described in
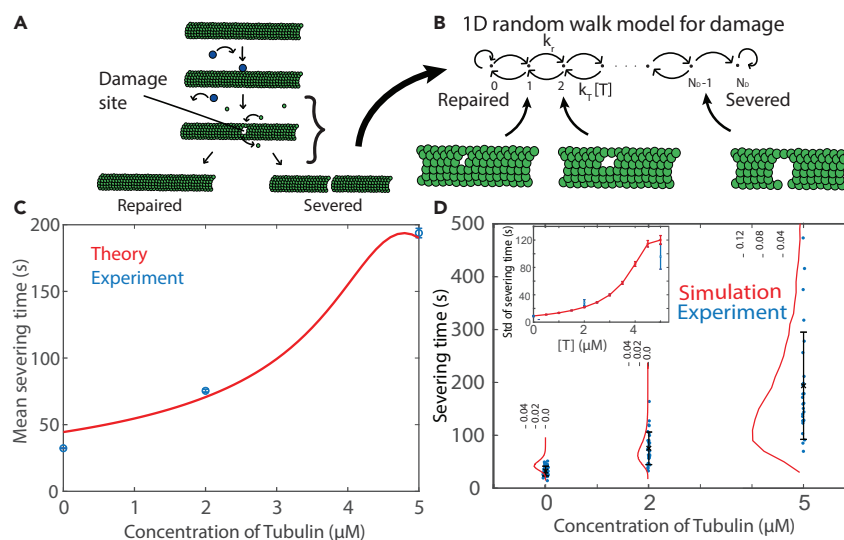
Figure 1. Microtubule severing with repair

(A) Severing proteins (in blue) create small damages on microtubule lattice which either get repaired by free tubulin or lose enough subunits to sever the microtubule.

(B) One-dimensional random walk model for studying the competition between removal of tubulin subunits at a rate k_r and the addition of subunits at a rate proportional to the free tubulin concentration, $k_T[T]$.

(C) We use published data[20] for the severing times as a function of tubulin concentration to estimate parameters of the severing model, which are listed in Table 1 (Figure S1).

(D) The same parameters are used to compute the standard deviation (inset) and probability distribution of severing time using stochastic simulations. Each distribution was computed from 400,000 trajectories. Error bars on experimental data obtained by bootstrapping method (in STAR methods). The error bars on the standard deviation from simulations show SEM calculated from 750 values, with each value computed from 20,000 trajectories. Comparison with published experimental data from ref.[20,] in blue is shown (Figure S2).

STAR methods), and the mean time it would take to sever a filament as a function of model parameters (k_T, k_r, and N_D). These calculations map to the classic first passage problem in physics[65] which has also found applications in many other contexts.[66]

Assuming an initial damage size of one subunit, and defining the ratio of the tubulin addition and removal rate as a dimensionless tubulin concentration $\tilde{T} = \frac{k_T[T]}{k_r}$, we predict that the time to sever a filament has the following form ($\tilde{T} \neq 1$)

$$T_{sev}(k_T, k_r, N_D) = \left(\frac{\frac{1}{k_r}}{\tilde{T} - 1} \right) \left(N_D \frac{(\tilde{T}^{N_D} + 1)}{(\tilde{T}^{N_D} - 1)} - \frac{\tilde{T} + 1}{\tilde{T} - 1} \right)$$

(Equation 1)

In the case, $\tilde{T} = 1$, $T_{sev}(k_T, k_r, N_D) = \frac{1}{6k_r}(N_D^2 - 1)$. (See STAR methods).

Considering the situation when the damage size that leads to severing $N_D \gg 1$, Equation 1 has two limits. When the rate of tubulin removal is greater than the rate of tubulin addition, i.e., $\tilde{T} \ll 1$, $T_{sev}(k_T, k_r, N_D) \approx \frac{N_D}{k_r}(1 + \tilde{T})$; the severing time is linear in tubulin concentration. When $\tilde{T} \gg 1$, $T_{sev}(k_T, k_r, N_D) \approx \left(\frac{N_D}{k_r} \frac{1}{\tilde{T}} \right)$, the severing time decreases as tubulin concentration increases. These limits indicate that there is a critical concentration of tubulin, $[T]_c = \frac{k_r}{k_T}$, which simply delineates different functional dependencies of the severing time on the concentration of free tubulin. We also note that the severing timescale is given by $\frac{N_D}{k_r}$, which is the mean time for completing N_D tubulin removal steps, each lasting $\frac{1}{k_r}$, on average. Equation 1 was checked against stochastic simulation of severing with repair (described in STAR methods and Figure S3).

Next, we use published data to estimate the parameters of our model of severing with repair. We consider the measured probability to sever and severing time as a function of tubulin concentration published in Figures 3D and 3H in ref. [20] and fit our model parameters (k_T, k_r, and N_D) using the method of least squares, described in STAR methods; see Figure 1C. The sensitivity of our results on the chosen parameters is shown in Figure S1. Using the estimated parameters, listed in Table 1, we conduct stochastic simulations of the model (see STAR methods and Figure S1 in the SI) to compute the distribution of severing times as a function of tubulin concentration and compare it to published data. Notably, just as in the published data,[20] we find that the distribution of severing times is asymmetric around the maximum and skewed toward large times; see Figures 1D and S2. A quantitative comparison between the measured standard deviation of the severing time and the prediction from our model is shown in the inset of Figure 1D.

Table 1. Parameters used in the models for the model of severing and length control with tubulin-induced repair

Parameters	Value used in paper	Reference
Concentration of Tubulin, [T]	0-5 μM	Vemu et al.[20]
Rate of replenishment, k_T	0.11 μM^{-1}s^{-1}	Estimated
Rate of removal, k_r	0.54 s^{-1}	Estimated
Minimum size of damage	1 monomer	Assumed
Maximum size of damage N_D	25	Estimated
Rate of growth, k	3.4 μM^{-1}s^{-1}	Mickolajczyk et al.[67]
Concentration of severing proteins, [S]	50 nM	Vemu et al.[20]
Severing protein landing rate, k_d	0.002 μM^{-1}s^{-1}nm^{-1}	Kuo et al.[48]

Estimated values were attained by fitting the theoretical expression for the mean severing time to experimental data in ref.[20]; see Figure 1C.

The published experiment[20] suggests that severing time is monotonic in the tubulin concentration up to 5 μM. Interestingly, our model (Equation 1) predicts a non-monotonic relationship between severing time and the concentration of tubulin (see Figure 2A). We find, as reported in the study, that severing time increases as the concentration of tubulin is increased but only until a certain critical concentration of tubulin. Above this concentration, as shown in Equation 1, we predict that the severing time should decrease. This model prediction of non-monotonicity of severing time needs to be validated.

The probability of severing is the probability that the one-dimensional random walker reaches the $x = N_D$ boundary before the $x = 0$ boundary:

$$P_{sev}([T]) = \frac{\tilde{T} - 1}{\tilde{T}^{N_D} - 1}, \qquad \text{(Equation 2)}$$

where we have chosen the initial damage size of 1, while N_D is the damage size that produces a severing event, and we expect $N_D \gg 1$ (see Table 1). Again, this expression has two limits (shown in dotted black lines in Figure 2): when $\tilde{T} < 1$, ($[T] < [T]_c$), $P_{sev}([T]) \approx 1 - \tilde{T}$, whereas when $\tilde{T} > 1$, $P_{sev}([T]) \approx \left(\frac{1}{\tilde{T}}\right)^{N_D - 1}$. Thus, above the critical concentration, the probability of severing is very small, almost all damages are likely to quickly be repaired by the free tubulin. With increasing tubulin concentration, the event of the initial damage to progressing to a severing event is unlikely and can only occur only if it happens in less time than the time to repair.

We confirmed our analytical expression for the mean severing time (Equation 1) and the probability of severing (Equation 2) as a function of tubulin concentration by stochastic simulations (See Figure S3).

Note that the fact that the waiting time for an "absorption event" decreases with increasing probability of removal has been discussed before in the context of escape problems in complex environments.[68] In this particular case, the non-monotonicity in the severing time (here due to the repair) is a prediction of the model that can be used to experimentally test the mechanism of severing with repair.

Length control in the presence of repair

The process of severing is a length-dependent disassembly mechanism wherein longer filaments are more likely to be severed. This results in negative feedback of filament length on a growing filament and leads to the control of length of cytoskeletal filaments.[54] Given the observation that damages created by severing proteins can be repaired by free tubulin,[20] we next ask how repair affects the length-control function of severing proteins.

Most microtubule-based structures in cells have microtubules growing from a nucleator, such as centrosome for a spindle, and centrioles for cilium. To account for this we consider a model of a single microtubule growing from a nucleating site, whose assembly rate is proportional to the concentration of free tubulin in the cytoplasm, and is subjected to severing by a severing protein (Figure 3A). We assume that both the free concentration of tubulin and the concentration of severing protein are constant in the cell. A severing event produces two microtubule fragments and we only follow the fate of the one that remains attached to the nucleator. The key question we address is how the length distribution of this microtubule, attached to the nucleator, is affected by tubulin-induced repair, which thus far has only been observed *in vitro*.[20] While microtubule-based structures such as cilia and spindles are composed of many individual microtubules, the length of individual filaments directly effects the size of the whole structure.[69]

Dynamic instability, steady microtubule assembly interspersed with rapid disassembly events called catastrophes, is a feature of microtubule filament dynamics *in vitro*.[10] Dynamic instability has also been recorded *in vivo*,[70] even though in microtubule-based structures such as cilia, catastrophes have not been observed. Furthermore, several microtubule-associated proteins, such as Kip2 and tau, reduce the rate of catastrophe.[71] Therefore, we analyze here dynamics of microtubules in the presence of severing, both without and with dynamic instability (see STAR methods, and Figure S6). We find that our main results about the effect of tubulin-induced repair on the steady-state microtubule length are qualitatively the same, whether we include dynamic instability or not. Additionally, ignoring dynamic instability makes the model analytically tractable.
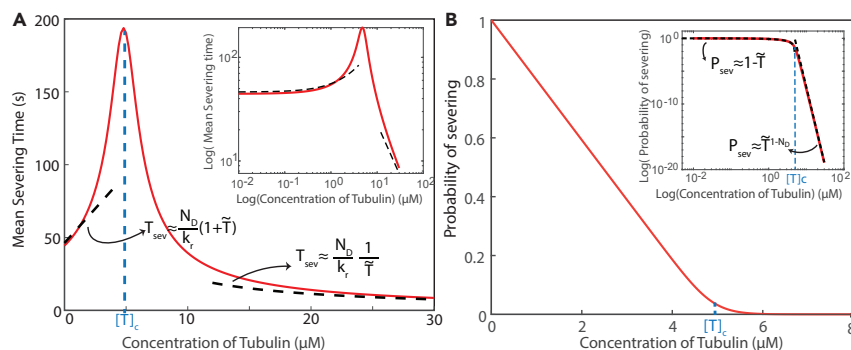
Figure 2. Theoretical prediction for model for microtubule severing with repair

(A) The model predicts a non-monotonic relationship between severing time and free tubulin concentration (Inset: plot on a log scale) and the existence of a critical concentration of tubulin, $[T]_c$, beyond which severing time decreases.

(B) Probability of severing decreases as the tubulin concentration is increased (Inset: plot on a log scale). The dashed lines in both plots show the asymptotic behavior at large $[T] \gg [T]_c$ and small $[T] \ll [T]_c$ free tubulin concentrations. Parameters used to plot these graphs are listed in Table 1.

When considering the effect of tubulin-induced repair on the assembly dynamics of microtubules at least two time scales need to be kept in mind: one is the time between consecutive damage creation events, due to different severing proteins landing on the side of a microtubule, and the time it takes to complete severing. First, we consider the situation when the severing timescale is very short and can be ignored. In this limit we obtain analytic results, which we test using stochastic simulations. In the case when the severing time cannot be ignored, we employ stochastic simulations, and reach similar conclusions as in the simpler case.

Using the computational scheme described in the STAR methods, we conduct stochastic simulations of the filament length as a function of time and analyze the process with and without the repair of severing protein induced damage (Figure 3A). In our simulations, individual filaments grow at a rate proportional to the tubulin concentration, $k\,[T]$, where k is the second order rate constant for the tubulin binding to the end of microtubules and has the units of $(\mu M.s)^{-1}$. Severing proteins land on the side of the filament with a rate proportional to the concentration of severing proteins $[S]$ and to the length of the filament, L. For the simulations without the repair process, severing along the filament proceeds with a rate $k_d[S]L$. In the simulation with the repair process, we take $k_d[S]L$ to represent the rate at which a damage site is created along the length of the microtubule. Assuming this is the rate limiting process in severing (i.e., ignoring the time to sever), the rate of severing can be written as $k_d[S]LP_{sev}$ where P_{sev} is the probability to sever (Equation 2).

For the two cases (severing without and severing with repair), we generate trajectories of length over time and notice that, after a steep growth phase, the filament length fluctuates around different steady-state lengths. We generate trajectories at three different tubulin concentrations and find that the mean lengths achieved by the filaments are much larger when the process of repair is included (Figure 3B). For the case, when severing times are assumed short and can be neglected, we also obtained analytic results for the mean filament length at steady state as $L_s^{without\ repair} = \sqrt{\frac{\pi k[T]}{2\,k_d[S]}}$, and $L_s^{with\ repair} = \sqrt{\frac{\pi k[T]}{2\,k_d[S]P_{sev}([T])}}$. These expressions were confirmed using simulations. As shown in Figure 3C, while the steady state length $L_s \sim \sqrt{[T]}$ without repair, we observe two regimes with tubulin-induced repair present – when $[T] < [T]_c$, $L_s \sim \sqrt{[T]}$ and when $[T] > [T]_c$, $L_s \sim [T]^{N_D/2}$, suggesting ultrasensitivity of the steady state microtubule length to tubulin concentration, when above the critical concentration (for details see STAR methods). It is to be noted that the model (with repair) is the same as the one (without repair) and differ only in the severing rate. In the event that Tubulin induced repair is not possible, then $P_{sev}([T]) = 1$ and the two models will give exactly the same behavior.

Note that our results for severing without repair (in particular the scaling result, $L_s \sim \sqrt{[T]/[S]}$) are qualitatively similar to the predictions for the "no catastrophe model" in a recently published paper which studied the effect of the severing protein spastin on microtubule length,[48] and tracked both parts of the microtubule after severing (Figure S4). We find that including the possibility of repair of severing events in our model predicts a new regime of microtubule dynamics that was not described previously in,[48] where the steady state length varies very strongly with the tubulin concentration, $L_s \sim [T]^{N_D/2}$.

To characterize the fluctuations of the microtubule length in steady state we calculated the coefficient of variation (CV = standard deviation/mean, commonly referred to as the noise) of the steady-state lengths, with and without repair. Significantly, we find that CV doesn't change with $[T]$ (See Figure 3D, inset and in STAR methods) even though the mean lengths are very different for the two models for $[T]$ above $[T]_c$. This results can be used to discern this mechanism from other control mechanisms from experiments that measure length fluctuations of cytoskeleton structures.[54,72]

So far we have ignored the time to sever assuming it is much shorter than the time between two consecutive damage-creating events, when severing proteins bind to the side of the microtubule and induce damage. When this assumption is no longer true several damage events can happen at once, before the microtubule is severed, and damage spreading can happen at multiple locations at once. In order to study the implications of this scenario, we performed stochastic simulations in which we tracked the locations of multiple damage sites
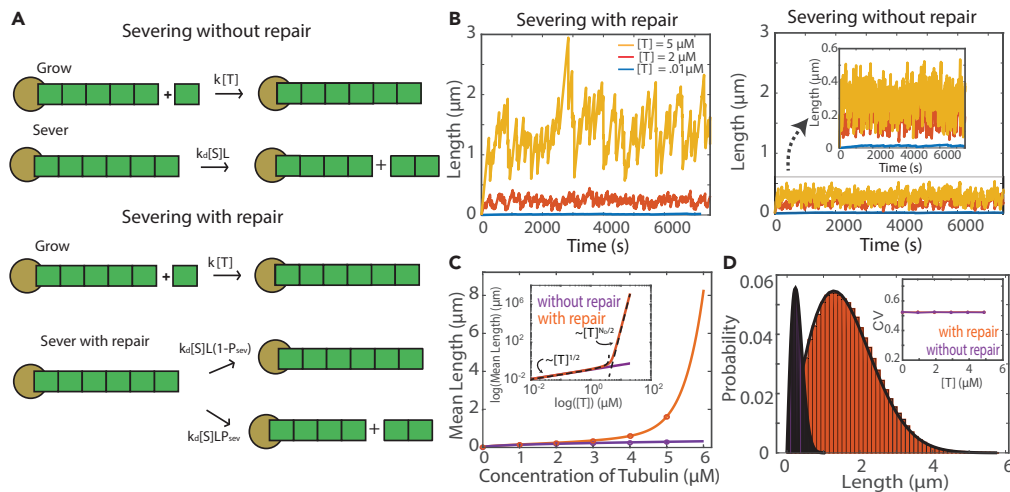
Figure 3. Effect of repair on microtubule filament length control via severing

(A) Schematic of the two models considered. Severing without repair: A microtubule filament (in green), attached to a nucleator (brown) grows with a rate $k[T]$ and is severed with a rate $k_d[S]L$, where L is the microtubule length. Severing with repair: Microtubule filaments grow with a rate $k[T]$ and either get severed with a rate $k_d[S]LP_{sev}$ or repaired with a rate $k_d[S]L(1 - P_{sev})$ where P_{sev} (probability of severing) is calculated using Equation 2. If severing occurs, the end portion of the filament (right part) is removed.

(B) Dynamics of filament length (average of 3 length trajectories shown for clarity) for the two models obtained using stochastic simulations. Dynamic range of the steady state filament lengths as [T] is tuned is larger with repair than without.

(C) Mean steady state length as a function of tubulin concentration (Log-Log plot inset). Dots are from simulations; lines are from analytic calculations for the model with repair (orange) and without (purple). The dashed lines represent the show the asymptotic behavior at large $[T] \gg [T]_c$ and small $[T] \ll [T]_c$.

(D) Distribution of steady state lengths and coefficient of variation (inset) as a function of tubulin concentration, each computed from 10^6 trajectories. Parameters in the steady-state simulations are listed in Table 1.

on a microtubule lattice (See in STAR methods and Figure S5). Each damage site has a corresponding severing time, drawn from a distribution of severing times obtained from the stochastic simulation of the damage spreading simulations.

When examining the steady state microtubule length in this case using simulations, we find results that are similar to what we obtained from the simple model above, in which we ignore both catastrophes and the time it takes to sever. In particular, we again observe the ultra-sensitive response of the steady state length to the change in the free tubulin concentration (see Figure S5). The fluctuations of the filament length in this case are different, and are characterized by a tubulin concentration dependent coefficient of variation (see Figure S5).

DISCUSSION

Dynamics of protein filaments in cells are very different from what is observed *in vitro*.[11] For example, actin networks in cells disassemble on the order of seconds whereas *in vitro* actin filaments disassemble over minutes.[7,8] These observations suggest that the dynamics of filament assembly are affected by proteins that associate with filaments *in vivo* and exert control over assembly and/or disassembly.[29,30,73] Inspired by recent experiments on microtubules,[20] we consider one such control system and demonstrate that it leads to dynamics that are distinct from those described for microtubules in isolation.

We model the severing of microtubules as a competition between the process of removal of subunits from the damage site created by a severing protein and the repair of the damage site by binding of free subunits. We use a one-dimensional random walk model of damage spreading to describe this competition and compute quantities that can be measured in experiments, such as the probability of severing, and the time taken to successfully sever a microtubule, as a function of the free tubulin concentration. We quantitatively compare our theory to a number of experimental observations[20] pertaining to the effect of severing proteins on microtubules. Notably, we predict a distribution of severing times (Figure 1D) skewed toward large severing times, which was observed in experimental results.[20] Additionally, using our model, we predict that the time to sever has a non-monotonic dependence on tubulin concentration and reaches a maximum at a critical tubulin concentration. Finally, we examined theoretically the implication of this repair process on the dynamics of a growing filament and found that it leads to a very sensitive dependence of the steady state filament length as a function of the free tubulin concentration.

Signatures of severing as a length-control mechanism

Often in cells, several mechanisms can be at play to control the size of a sub-cellular structure, making it challenging to distinguish between them. Key results of this paper can serve as quantitative signatures of the severing mechanism.

A key feature of length-control mechanisms is that they lead to a peaked distribution of steady-state filament lengths. Several theoretical and experimental studies have demonstrated that severing can control the length of filaments.[48,54,74] Longer microtubules have more binding

sites for severing proteins, and therefore have a greater probability of being severed than shorter ones. This leads to negative feedback on the length of a growing microtubule which eventually reaches a steady-state length once the disassembly rate balances the rate of assembly. The resulting distribution of steady-state lengths, in addition to being peaked, has a skewness (see Figure 3D) which makes it distinct from other control mechanisms studied thus far.[54] This skewness, predicted in theoretical studies,[48,54,55] was observed in recent experimental studies.[20,48] Additionally, we also find that the coefficient of variation (CV) of steady state microtubule lengths is independent of the concentration of tubulin and has a constant value equal to 0.523 (See Figure 3D inset and STAR methods). This result relies on an assumption that the severing process is uniform along the filament, as was recently reported for spastin.[48] Factors like tubulin glutamylation could invalidate this assumption,[75] as Spastin and katanin have been shown to have significantly higher severing rates on polyglutamylated microtubules or tyrosinated ones.[75,76] Additionally, Both spastin and katanin are also inhibited by MAPs[77,78] which form patches on microtubules. All of these factors can create uneven severing on a microtubule in a cellular setting.

Experimental predictions

Probability of severing as a function of tubulin concentration

We have shown that a one-dimensional random walk model quantitatively accounts for recent experiments on microtubule severing. Using this model, we find the probability of severing decreases as the concentration of tubulin increases (See Figure 2B). This prediction of the model can be used to further test it. Many studies have used a "severing assay" to study the effect of severing proteins on microtubules.[20,44,45,79,80] In these experiments, severing proteins are flown into a reaction chamber with pre-formed microtubules and quantities like the number of successful severing events per unit length of the microtubule (the severing rate) can thus be measured. Note that the maximal rate of severing is achieved when there is no free tubulin to repair the initial damage caused by a severing protein. Therefore, the ratio of the severing rate in the presence of free tubulin to the severing rate with no free tubulin is the probability of severing. At zero concentration of free tubulin, we expect that all severing initiation events lead to successful severing, but that the proportion would decrease as free tubulin can lead to repair, which is captured by Equation 2, and Figure 2B. Interestingly, this prediction of the probability of severing decreasing with the increase in free tubulin concentration has already been observed by some studies.[20,44,45]

Non-monotonic relationship of severing time and free tubulin concentration

Importantly, our model predicts a critical tubulin concentration $[T]_c = k_r/k_T$, where k_r is the first order rate of removal and k_T is the second order rate of addition of tubulin from the damage site. Above this critical concentration, the probability of severing drops rapidly, causing the severing time to peak at $[T]_c$; see Figure 2A. By using our estimated parameters, we predict that the mean severing time should increase for $0 \leq [T] \leq 5\mu M$, a prediction which agrees with results from experiments described in a recent study[20] and also observed in ref.[45] However, at tubulin concentrations above those which were experimentally investigated in ref.[20] i.e., $[T] > 5\mu M$, our model predicts that severing time should decreases. This prediction can be used to test the model using the set-up described in studies.[20,45]

We also note that although our study here is focused on tubulin-induced repair at damages created by severing proteins on microtubules, our model of damage spreading may be useful for analyzing other situations where reincorporation of new tubulin on a microtubule shaft has been observed, such as at sites of defects created by mechanical stress[46,56] or motor protein-induced damage[49,50] on microtubules.

Ultrasensitivity of microtubule length control

Ultrasensitivity in living systems is usually defined in terms of an input-output function with the property that the output varies strongly, for example as a large power, of one or more of its inputs.[81] Examples of such ultrasensitivity can be found in signaling networks and also in the cooperative assembly of large complexes, such as viruses.[82] Here, as shown in Figure 3C (where $L_s \sim [T]^{N_D/2}$ when $[T] > [T]_c$) we describe the ultrasensitive response of the microtubule length (the output) to changes in free tubulin concentration (the input) when the length is controlled by severing where the severing process proceeds by tubulin dependent spreading of damage to the tubulin lattice induced by the binding of a severing protein.

In Figure 4, we show results of calculations of the steady-state length (L_S) and the coefficient of variation as a function of two experimentally tunable knobs – tubulin and severing protein concentrations. We find a sharp increase in L_S with $[T]$ above the critical concentration $[T]_c = \frac{k_r}{k_T}$, while the coefficient of variation remains the same across all concentrations of severing proteins. These results can be tested by creating an *in vitro* system[20,28,36] in which growing microtubules are exposed to severing proteins. We also compute the probability distribution of steady-state lengths as a function of tubulin concentrations which can be used as a more stringent test of the model (see Figure 3D).

Examining the assumptions of the model

In order to make the model of severing with repair analytically tractable, we made a few simplifying assumptions. Below we examine how robust our conclusions are with respect to these assumptions.

Effect of finite severing time on microtubule dynamics

In our calculations of microtubule length-control (Figures 3 and 4), we ignore the time it takes for the severing event to complete once the initial damage is created. This is equivalent to assuming that the time between subsequent damage creation events is much bigger than
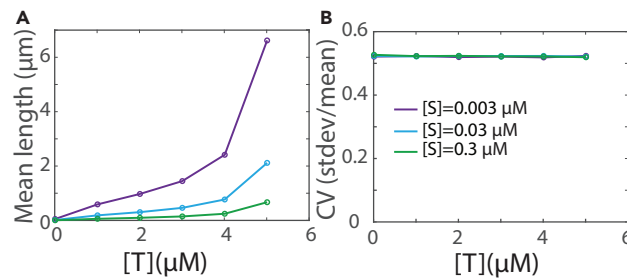
Figure 4. Experimentally testable predictions of the severing with repair model of length control
(A) Mean filament length and (B) coefficient of variation at steady state as function of Tubulin concentration at different severing protein concentrations. Dynamic range is larger at lower concentrations of severing proteins, and the coefficient of variation is independent of tubulin and severing protein concentrations. Parameters used in the simulation are listed in Table 1.

time to sever. This is a reasonable assumption in the limits of low and high tubulin concentrations, but not a valid one for intermediate tubulin concentrations (Figure S5 and STAR methods).

Using the rates in Table 1, for small tubulin concentrations $[T] \approx 0.01 \mu M$, typical microtubules lengths are small, about 50 nm (using equation $L_s \sim \sqrt{\frac{\pi k[T]}{2 k_d[S]}}$ at small $[T]$ approximation) and $P_{sev}[T]$ is close to 1, which means practically all damage events lead to severing. Time taken for a severing protein to bind to a microtubule and induce damage is $\approx \frac{1}{k_d[S]L} = 200s$ for a microtubule of length around 50 nm. In comparison, the severing time after initial damage $\approx \frac{N_D}{k_r} = 50 \ secs$. Thus, at low tubulin concentrations, severing time is shorter than the severing protein binding time, making it unlikely that multiple damage sites are created. At high tubulin concentrations $[T] > 5 \ \mu M$, the microtubules are > 1 micron in length, and the time for a severing protein to bind is around 10 s. At these tubulin concentrations, the probability of severing is small ($\lesssim 0.025$) and on average, at least 40 binding events are required for one severing event. Waiting time for 40 binding events is about 400 s, which is greater than the severing time (200s or less) (Figure S5D, inset). Thus, our simplified model that ignores the possibility of multiple damage sites, in addition to being analytically tractable, provides a good approximation to study the effect of severing on microtubule length control in the limits of low and high tubulin concentrations.

At intermediate tubulin concentrations, however, time between severing events is comparable to severing time (Figure S5D, inset), making it possible that several damage events are happening at once. This can lead to correlations between severing events which our calculations ignore. In order to study the implications of this scenario, we performed stochastic simulations wherein we tracked the locations of multiple damage sites on a microtubule lattice. Each damage site has a corresponding severing time, drawn from a distribution of severing times obtained from the stochastic simulation of the damage spreading simulations (described in STAR methods and Figure S5). We observe that results of large dynamic range in steady-state length from this simulation are similar to what was seen with the simple model (Figures 3C and S5). Additionally, the noise as a function of free tubulin concentration from the full simulation was identical to the one obtained from the simple model at low and high tubulin concentration. However, at intermediate values of tubulin concentrations, we notice a peak in the CV vs. tubulin concentration plot (Figure S5D), which was in contrast to the constant value seen with the simple model (Figure S5) but to be expected due to correlations in severing events.

Dynamic instability

Microtubules are known to switch between phases of slow growth and rapid shrinking by a process known as dynamic instability. The rates of switching from shrinking to growth and vice versa are called rates of rescue and catastrophe, respectively. In our simulations leading to Figures 3 and 4, we assumed that the microtubule are stabilized, and are not undergoing dynamic instability. In order to check the robustness of our results, we included dynamic instability in our simulations (see in STAR methods for simulation protocol). We found that dynamic instability did not qualitatively change the observation of large dynamic range of filament lengths. Coincidentally, a previous theoretical study analyzed the effect of the severing protein spastin on dynamic microtubules, and reported that their model predictions were similar to a model which ignored the dynamic instability ("no catastrophe" model).[48]

With stabilized microtubules, we had calculated that the coefficient of variation (CV) for the steady state length fluctuations for the models of severing without repair and severing with repair was constant with respect to tubulin concentration. In contrast, when dynamic instability was included, we observed a non-monotonic relationship in CV for both models (see Figure S6). In our simulations, microtubule filaments grow at a rate proportional to tubulin concentration. Since severing depends on microtubule length, which is typically small at low concentrations of tubulin, dynamic instability dominates over severing in both models. In this regime, the length distributions are exponential and resulting in CV being close to one.[28,83] However, we observe different behaviors for both models (severing without repair and severing with repair) at higher tubulin concentration. In this regime, filaments grow longer and severing dominates over dynamic instability, as the number of subunits lost in a catastrophe event is small compared to the number of subunits lost due to severing. So, as expected, in the model of severing without repair, CV converges toward 0.523 at large concentration of tubulin. In severing with repair, we observe that CV shows a non-monotonic behavior with tubulin concentration, where it first decreases and then increases, and the dip in CV depends on the rescue

rates chosen. Additionally, *in-vitro* studies have reported an increase in rescue rates in presence of severing proteins. Several hypotheses have been proposed to explain this, such as, the incorporation of new tubulin creating a "GTP-island", which promotes rescue[20] and the accumulation of severing proteins on the tips of shrinking microtubules, where they slow shrinkage and promote rescue.[28] At this point, it is unknown whether severing proteins have the same effect *in vivo*, where they may interact with other microtubule associated proteins. For example, studies have reported that molecular motor kinesin-1 can damage the microtubule shaft and induce incorporation of GTP-tubulin,[50,51] thus increasing probability of rescue and affecting microtubule length and stability.[17]

In summary, our calculations show that tubulin and severing proteins can cause qualitatively new dynamics of microtubules. Using simulations and theory, our study describes the role of a free pool of building blocks on the process of repair of damage created by severing proteins and its implications for the control of length of microtubules. Here we show the existence of a critical tubulin concentration above which severing becomes strongly dependent on $[T]$, leading to a rare but fast severing. We find that microtubule length control via severing with tubulin-induced repair is ultra-sensitive to changes in the concentrations of tubulin leading to a dramatically increased dynamic range of filament lengths at steady state. This mechanism may have biological significance in processes like mitotic spindle size scaling during development where relatively small changes in microtubule growth rates have been correlated with large changes in mitotic spindle size.[84] Our study shows how the antagonistic action of assembly and disassembly factors can influence dynamical properties of microtubules.

Limitations of the study

We made several simplifying assumptions in our models of damage spreading and severing protein mediated length-control. The guiding principle behind these assumptions is to make simple models with a few parameters that make quantitative predictions for experiments, which can be tested. In our damage spreading model, we assume that the rates of adding or removing a tubulin dimer, which increase or decrease the size of the damaged region, do not depend on the size or geometry of the damaged region. We also assume that the rate of severing is uniform along the length of the microtubule, which may not be true in cellular environments due to the presence of other microtubule associated proteins. To the extent that future experiments falsify the key quantitative predictions of our models these assumptions will have to be revisited, and in doing so we hope other relevant contributions to the severing dynamics will be revealed.

STAR★METHODS

Detailed methods are provided in the online version of this paper and include the following:

- KEY RESOURCES TABLE
- RESOURCE AVAILABILITY
  - Lead contact
  - Materials availability
  - Data and code availability
- METHOD DETAILS
  - Calculation of probability of severing
  - Calculation for time to either sever or repair
  - Calculation of severing time
  - Calculation of probability distribution of filament lengths, due to severing with and without repair
- QUANTIFICATION AND STATISTICAL ANALYSIS
  - Estimation of parameters
  - Stochastic simulation schemes
  - Conversion between monomer number and filament length
  - Effect of finite severing time on microtubule dynamics
  - Effect of dynamic instability and severing on microtubule dynamics

SUPPLEMENTAL INFORMATION

Supplemental information can be found online at https://doi.org/10.1016/j.isci.2024.108874.

REFERENCES

1. Song, L., and Dentler, W.L. (2001). Flagellar Protein Dynamics in Chlamydomonas. J. Biol. Chem. *276*, 29754–29763.

2. Marshall, W.F., Qin, H., Rodrigo Brenni, M., and Rosenbaum, J.L. (2005). Flagellar length control system: testing a simple model based on intraflagellar transport and turnover. Mol. Biol. Cell *16*, 270–278.

3. Bennabi, I., Terret, M.-E., and Verlhac, M.-H. (2016). Meiotic spindle assembly and chromosome segregation in oocytes. J. Cell Biol. *215*, 611–619.

4. Hyman, A.A., and Karsenti, E. (1996). Morphogenetic Properties of Microtubules and Mitotic Spindle Assembly. Cell *84*, 401–410.

5. Dumont, S., and Mitchison, T.J. (2009). Force and length in the mitotic spindle. Curr. Biol. *19*, R749–R761.

6. Pollard, T.D. (1986). Rate constants for the reactions of ATP- and ADP-actin with the ends of actin filaments. J. Cell Biol. *103*, 2747–2754.

7. Watanabe, N., and Mitchison, T.J. (2002). Single-molecule speckle analysis of actin filament turnover in lamellipodia. Science *295*, 1083–1086.

8. Miyoshi, T., and Watanabe, N. (2013). Can filament treadmilling alone account for the F-actin turnover in lamellipodia? Cytoskeleton *70*, 179–190.

9. Kuhn, J.R., and Pollard, T.D. (2005). Real-time measurements of actin filament polymerization by total internal reflection fluorescence microscopy. Biophys. J. *88*, 1387–1402.

10. Desai, A., and Mitchison, T.J. (1997). Microtubule polymerization dynamics. Annu. Rev. Cell Dev. Biol. *13*, 83–117.

11. Zwetsloot, A.J., Tut, G., and Straube, A. (2018). Measuring microtubule dynamics. Essays Biochem. *62*, 725–735.

12. Desai, A., Verma, S., Mitchison, T.J., and Walczak, C.E. (1999). Kin I Kinesins Are Microtubule-Destabilizing Enzymes. Cell *96*, 69–78.

13. Gardner, M.K., Zanic, M., and Howard, J. (2013). Microtubule Catastrophe and Rescue. Curr. Opin. Cell Biol. *25*, 14–22.

14. Geisterfer, Z.M., Zhu, D.Y., Mitchison, T.J., Oakey, J., and Gatlin, J.C. (2020). Microtubule Growth Rates Are Sensitive to Global and Local Changes in Microtubule Plus-End Density. Curr. Biol. *30*, 3016–3023.e3.

15. Goshima, G., Wollman, R., Stuurman, N., Scholey, J.M., and Vale, R.D. (2005). Length control of the metaphase spindle. Curr. Biol. *15*, 1979–1988.

16. Tournebize, R., Popov, A., Kinoshita, K., Ashford, A.J., Rybina, S., Pozniakovsky, A., Mayer, T.U., Walczak, C.E., Karsenti, E., and Hyman, A.A. (2000). Control of microtubule dynamics by the antagonistic activities of XMAP215 and XKCM1 in Xenopus egg extracts. Nat. Cell Biol. *2*, 13–19.

17. Schaer, J., Andreu-Carbó, M., Kruse, K., and Aumeier, C. (2023). The effect of motor-induced shaft dynamics on microtubule stability and length. Biophys. J. *122*, 346–359.

18. Shekhar, S., Chung, J., Kondev, J., Gelles, J., and Goode, B.L. (2019). Synergy between Cyclase-associated protein and Cofilin accelerates actin filament depolymerization by two orders of magnitude. Nat. Commun. *10*, 5319.

19. Arpağ, G., Lawrence, E.J., Farmer, V.J., Hall, S.L., and Zanic, M. (2020). Collective effects of XMAP215, EB1, CLASP2, and MCAK lead to robust microtubule treadmilling. Proc. Natl. Acad. Sci. USA *117*, 12847–12855.

20. Vemu, A., Szczesna, E., Zehr, E.A., Spector, J.O., Grigorieff, N., Deaconescu, A.M., and Roll-Mecak, A. (2018). Severing enzymes amplify microtubule arrays through lattice GTP-tubulin incorporation. Science *361*, eaau1504.

21. King, M.R., and Petry, S. (2020). Phase separation of TPX2 enhances and spatially coordinates microtubule nucleation. Nat. Commun. *11*, 270.

22. Ohi, R., Strothman, C., and Zanic, M. (2021). Impact of the 'tubulin economy' on the formation and function of the microtubule cytoskeleton. Curr. Opin. Cell Biol. *68*, 81–89.

23. Woodruff, J.B., Ferreira Gomes, B., Widlund, P.O., Mahamid, J., Honigmann, A., and Hyman, A.A. (2017). The Centrosome Is a Selective Condensate that Nucleates Microtubules by Concentrating Tubulin. Cell *169*, 1066–1077.e10.

24. Van Geel, O., Cheung, S., and Gadella, T.W.J. (2020). Combining optogenetics with sensitive FRET imaging to monitor local microtubule manipulations. Sci. Rep. *10*, 6034.

25. Walczak, C.E., Gayek, S., and Ohi, R. (2013). Microtubule-Depolymerizing Kinesins. Annu. Rev. Cell Dev. Biol. *29*, 417–441.

26. Arellano-Santoyo, H., Geyer, E.A., Stokasimov, E., Chen, G.-Y., Su, X., Hancock, W., Rice, L.M., and Pellman, D. (2017). A Tubulin Binding Switch Underlies Kip3/Kinesin-8 Depolymerase Activity. Dev. Cell *42*, 37–51.e8.

27. Varga, V., Leduc, C., Bormuth, V., Diez, S., and Howard, J. (2009). Kinesin-8 motors act cooperatively to mediate length-dependent microtubule depolymerization. Cell *138*, 1174–1183.

28. Kuo, Y.-W., Trottier, O., Mahamdeh, M., and Howard, J. (2019). Spastin is a dual-function enzyme that severs microtubules and promotes their regrowth to increase the number and mass of microtubules. Proc. Natl. Acad. Sci. USA *116*, 5533–5541.

29. Kuo, Y.-W., and Howard, J. (2021). Cutting, Amplifying, and Aligning Microtubules with Severing Enzymes. Trends Cell Biol. *31*, 50–61.

30. Sharp, D.J., and Ross, J.L. (2012). Microtubule-severing enzymes at the cutting edge. J. Cell Sci. *125*, 2561–2569.

31. Sarbanes, S.L., Zehr, E.A., and Roll-Mecak, A. (2022). Microtubule-severing enzymes. Curr. Biol. *32*, R992–R997.

32. Vale, R.D. (1991). Severing of stable microtubules by a mitotically activated protein in xenopus egg extracts. Cell *64*, 827–839.

33. Evans, K.J., Gomes, E.R., Reisenweber, S.M., Gundersen, G.G., and Lauring, B.P. (2005). Linking axonal degeneration to microtubule remodeling by Spastin-mediated microtubule severing. J. Cell Biol. *168*, 599–606.

34. Roll-Mecak, A., and Vale, R.D. (2005). The Drosophila homologue of the hereditary spastic paraplegia protein, spastin, severs and disassembles microtubules. Curr. Biol. *15*, 650–655.

35. Mukherjee, S., Diaz Valencia, J.D., Stewman, S., Metz, J., Monnier, S., Rath, U., Asenjo, A.B., Charafeddine, R.A., Sosa, H.J., Ross, J.L., et al. (2012). Human Fidgetin is a microtubule severing the enzyme and minus-end depolymerase that regulates mitosis. Cell Cycle *11*, 2359–2366.

36. Díaz-Valencia, J.D., Morelli, M.M., Bailey, M., Zhang, D., Sharp, D.J., and Ross, J.L. (2011). Drosophila Katanin-60 Depolymerizes and Severs at Microtubule Defects. Biophys. J. *100*, 2440–2449.

37. Chaudhry, F., Breitsprecher, D., Little, K., Sharov, G., Sokolova, O., and Goode, B.L. (2013). Srv2/cyclase-associated protein forms hexameric shurikens that directly catalyze actin filament severing by cofilin. Mol. Biol. Cell *24*, 31–41.

38. Balcer, H.I., Goodman, A.L., Rodal, A.A., Smith, E., Kugler, J., Heuser, J.E., and Goode, B.L. (2003). Coordinated regulation of actin filament turnover by a high-molecular-weight Srv2/CAP complex, cofilin, profilin, and Aip1. Curr. Biol. *13*, 2159–2169.

39. Johnston, A.B., Collins, A., and Goode, B.L. (2015). High-speed depolymerization at actin

filament ends jointly catalysed by Twinfilin and Srv2/CAP. Nat. Cell Biol. *17*, 1504–1511.

40. Loughlin, R., Wilbur, J.D., McNally, F.J., Nédélec, F.J., and Heald, R. (2011). Katanin Contributes to Interspecies Spindle Length Scaling in Xenopus. Cell *147*, 1397–1407.

41. Karabay, A., Yu, W., Solowska, J.M., Baird, D.H., and Baas, P.W. (2004). Axonal growth is sensitive to the levels of katanin, a protein that severs microtubules. J. Neurosci. *24*, 5778–5788.

42. Ahmad, F.J., Yu, W., McNally, F.J., and Baas, P.W. (1999). An Essential Role for Katanin in Severing Microtubules in the Neuron. J. Cell Biol. *145*, 305–315.

43. Jinushi-Nakao, S., Arvind, R., Amikura, R., Kinameri, E., Liu, A.W., and Moore, A.W. (2007). Knot/Collier and Cut Control Different Aspects of Dendrite Cytoskeleton and Synergize to Define Final Arbor Shape. Neuron *56*, 963–978.

44. Bailey, M.E., Sackett, D.L., and Ross, J.L. (2015). Katanin Severing and Binding Microtubules Are Inhibited by Tubulin Carboxy Tails. Biophys. J. *109*, 2546–2561.

45. Reuther, C., Santos-Otte, P., Grover, R., Heldt, G., Woehlke, G., and Diez, S. (2022). Multiplication of Motor-Driven Microtubules for Nanotechnological Applications. Nano Lett. *22*, 926–934.

46. Aumeier, C., Schaedel, L., Gaillard, J., John, K., Blanchoin, L., and Théry, M. (2016). Self-repair promotes microtubule rescue. Nat. Cell Biol. *18*, 1054–1064.

47. Schaedel, L., John, K., Gaillard, J., Nachury, M.V., Blanchoin, L., and Théry, M. (2015). Microtubules self-repair in response to mechanical stress. Nat. Mater. *14*, 1156–1163.

48. Kuo, Y.-W., Trottier, O., and Howard, J. (2019). Predicted Effects of Severing Enzymes on the Length Distribution and Total Mass of Microtubules. Biophys. J. *117*, 2066–2078.

49. Sen, A., and Kunwar, A. (2023). Computer simulation reveals the effect of severing enzymes on dynamic and stabilized microtubules. Phys. Biol. *20*, 036002.

50. Triclin, S., Inoue, D., Gaillard, J., Htet, Z.M., DeSantis, M.E., Portran, D., Derivery, E., Aumeier, C., Schaedel, L., John, K., et al. (2021). Self-repair protects microtubules from destruction by molecular motors. Nat. Mater. *20*, 883–891.

51. Andreu-Carbó, M., Fernandes, S., Velluz, M.-C., Kruse, K., and Aumeier, C. (2022). Motor usage imprints microtubule stability along the shaft. Dev. Cell *57*, 5–18.e8.

52. Berg, H.C. (1993). Random Walks in Biology (Princeton University Press).

53. Roland, J., Berro, J., Michelot, A., Blanchoin, L., and Martiel, J.-L. (2008). Stochastic Severing of Actin Filaments by Actin Depolymerizing Factor/Cofilin Controls the Emergence of a Steady Dynamical Regime. Biophys. J. *94*, 2082–2094.

54. Mohapatra, L., Goode, B.L., Jelenkovic, P., Phillips, R., and Kondev, J. (2016). Design Principles of Length Control of Cytoskeletal Structures. Annu. Rev. Biophys. *45*, 85–116.

55. Tindemans, S.H., and Mulder, B.M. (2010). Microtubule length distributions in the presence of protein-induced severing. Phys. Rev. E *81*, 031910.

56. Schaedel, L., Triclin, S., Chrétien, D., Abrieu, A., Aumeier, C., Gaillard, J., Blanchoin, L., Théry, M., and John, K. (2019). Lattice defects induce microtubule self-renewal. Nat. Phys. *15*, 830–838.

57. Marshall, W.F., and Rosenbaum, J.L. (2001). Intraflagellar transport balances continuous turnover of outer doublet microtubules: implications for flagellar length control. J. Cell Biol. *155*, 405–414.

58. Ishikawa, H., and Marshall, W.F. (2011). Ciliogenesis: building the cell's antenna. Nat. Rev. Mol. Cell Biol. *12*, 222–234.

59. Hagen, K.D., McInally, S.G., Hilton, N.D., and Dawson, S.C. (2020). Microtubule organelles in Giardia. Adv. Parasitol. *107*, 25–96.

60. Dawson, S.C., and House, S.A. (2010). Imaging and analysis of the microtubule cytoskeleton in giardia. Methods Cell Biol. *97*, 307–339.

61. Decker, F., Oriola, D., Dalton, B., and Brugués, J. (2018). Autocatalytic microtubule nucleation determines the size and mass of Xenopus laevis egg extract spindles. Elife *7*, e31149.

62. Hendel, N.L., Thomson, M., and Marshall, W.F. (2018). Diffusion as a Ruler: Modeling Kinesin Diffusion as a Length Sensor for Intraflagellar Transport. Biophys. J. *114*, 663–674.

63. Fai, T.G., Mohapatra, L., Kar, P., Kondev, J., and Amir, A. (2019). Length regulation of multiple flagella that self-assemble from a shared pool of components. Elife *8*, e42599.

64. McInally, S.G., Kondev, J., and Dawson, S.C. (2019). Length-dependent disassembly maintains four different flagellar lengths in Giardia. Elife *8*, e48694.

65. Redner, S. (2001). A Guide to First-Passage Processes (Cambridge University Press).

66. Calef, D.F., and Deutch, J.M. (1983). Diffusion-Controlled Reactions. Annu. Rev. Phys. Chem. *34*, 493–524.

67. Mickolajczyk, K.J., Geyer, E.A., Kim, T., Rice, L.M., and Hancock, W.O. (2019). Direct observation of individual tubulin dimers binding to growing microtubules. Proc. Natl. Acad. Sci. USA *116*, 7314–7322.

68. Ma, J., Do, M., Le Gros, M.A., Peskin, C.S., Larabell, C.A., Mori, Y., and Isaacson, S.A. (2020). Strong intracellular signal inactivation produces sharper and more robust signaling from cell membrane to nucleus. PLoS Comput. Biol. *16*, e1008356.

69. Brugués, J., Nuzzo, V., Mazur, E., and Needleman, D.J. (2012). Nucleation and Transport Organize Microtubules in Metaphase Spindles. Cell *149*, 554–564.

70. Guo, Y., Li, D., Zhang, S., Yang, Y., Liu, J.-J., Wang, X., Liu, C., Milkie, D.E., Moore, R.P., Tulu, U.S., et al. (2018). Visualizing Intracellular Organelle and Cytoskeletal Interactions at Nanoscale Resolution on Millisecond Timescales. Cell *175*, 1430–1442.e17.

71. Bowne-Anderson, H., Hibbel, A., and Howard, J. (2015). Regulation of Microtubule Growth and Catastrophe: Unifying Theory and Experiment. Trends Cell Biol. *25*, 769–779.

72. Bauer, D., Ishikawa, H., Wemmer, K.A., Hendel, N.L., Kondev, J., and Marshall, W.F. (2021). Analysis of biological noise in the flagellar length control system. iScience *24*, 102354.

73. Zanic, M., Widlund, P.O., Hyman, A.A., and Howard, J. (2013). Synergy between XMAP215 and EB1 increases microtubule growth rates to physiological levels. Nat. Cell Biol. *15*, 688–693.

74. Roland, J., Berro, J., Michelot, A., Blanchoin, L., and Martiel, J.-L. (2008). Stochastic severing of actin filaments by actin depolymerizing factor/cofilin controls the emergence of a steady dynamical regime. Biophys. J. *94*, 2082–2094.

75. Valenstein, M.L., and Roll-Mecak, A. (2016). Graded Control of Microtubule Severing by Tubulin Glutamylation. Cell *164*, 911–921.

76. Szczesna, E., Zehr, E.A., Cummings, S.W., Szyk, A., Mahalingan, K.K., Li, Y., and Roll-Mecak, A. (2022). Combinatorial and antagonistic effects of tubulin glutamylation and glycylation on katanin microtubule severing. Dev. Cell *57*, 2497–2513.e6.

77. McNally, K.P., Buster, D., and McNally, F.J. (2002). Katanin-mediated microtubule severing can be regulated by multiple mechanisms. Cell Motil Cytoskeleton *53*, 337–349.

78. Siahaan, V., Krattenmacher, J., Hyman, A.A., Diez, S., Hernández-Vega, A., Lansky, Z., and Braun, M. (2019). Kinetically distinct phases of tau on microtubules regulate kinesin motors and severing enzymes. Nat. Cell Biol. *21*, 1086–1092.

79. Ziółkowska, N.E., and Roll-Mecak, A. (2013). In vitro microtubule severing assays. Methods Mol. Biol. *1046*, 323–334.

80. Belonogov, L., Bailey, M.E., Tyler, M.A., Kazemi, A., and Ross, J.L. (2019). Katanin catalyzes microtubule depolymerization independently of tubulin C-terminal tails. Cytoskeleton (Hoboken) *76*, 254–268.

81. Ferrell, J.E., and Ha, S.H. (2014). Ultrasensitivity part I: Michaelian responses and zero-order ultrasensitivity. Trends Biochem. Sci. *39*, 496–503.

82. Ferrell, J.E., and Ha, S.H. (2014). Ultrasensitivity part II: multisite phosphorylation, stoichiometric inhibitors, and positive feedback. Trends Biochem. Sci. *39*, 556–569.

83. Dogterom, M., and Leibler, S. (1993). Physical aspects of the growth and regulation of microtubule structures. Phys. Rev. Lett. *70*, 1347–1350.

84. Rieckhoff, E.M., Berndt, F., Elsner, M., Golfier, S., Decker, F., Ishihara, K., and Brugués, J. (2020). Spindle Scaling Is Governed by Cell Boundary Regulation of Microtubule Nucleation. Curr. Biol. *30*, 4973–4983.e10.

85. Margolin, G., Gregoretti, I.V., Cickovski, T.M., Li, C., Shi, W., Alber, M.S., and Goodson, H.V. (2012). The mechanisms of microtubule catastrophe and rescue: implications from analysis of a dimer-scale computational model. MBoC *23*, 642–656.

STAR★METHODS

KEY RESOURCES TABLE

REAGENT or RESOURCE	SOURCE	IDENTIFIER
Deposited data		
Experimental Data in Figures 1C and 1D	Vemu et al.,[20] Science 2018	https://www.science.org/doi/10.1126/science.aau1504
Software and algorithms		
MATLAB R2019a	MathWorks	https://www.mathworks.com/products/matlab.html?s_tid=hp_products_matlab
Codes to generate figures in the Main text and Supplementary materials	This paper	https://zenodo.org/doi/10.5281/zenodo.6622170
Wolfram Mathematica 13	Wolfram	https://www.wolfram.com/mathematica/

RESOURCE AVAILABILITY

Lead contact

Lishibanya Mohapatra (lxmsps@rit.edu)

Materials availability

This study did not generate new unique reagents.

Data and code availability

- This paper analyzes existing, publicly available data. These accession numbers for the datasets are listed in the key resources table.
- All original code has been deposited at Zenodo and is publicly available as of the date of publication. DOIs are listed in the key resources table.
- Any additional information required to reanalyze the data reported in this paper is available from the lead contact upon request.

METHOD DETAILS

Calculation of probability of severing

Here we apply ideas from "first-passage" problems in random walks (Redner, 2001[65], Calef and Deutch, 1983[66]) to understand the effect of tubulin-based repair on the severing process. The spreading of the damage to the tubulin lattice leading to a severing event is modeled as a random walk with absorbing boundary conditions.

We assume that once a severing protein lands on the side of a microtubule it creates a damage. This damage can spread or be repaired and size of the damage we describe by a one dimensional variable (x) that counts the number of missing tubulin-dimers at the site of damage. We assume that once a critical damage size ($x = N_D$) is reached the microtubule will fragment into two pieces. The fate of the damage is determined by a competition between the removal and addition of tubulin at the damage site, eventually leading to severing or repair as shown in Figure S3A in the SI. We assume that subunits are added to the damage site at a rate proportional to the concentration of free tubulin $k_T[T]$ (s^{-1}) and are removed from the damage site at a rate k_r (s^{-1}), with each step either increasing or decreasing the size of damage by 1. If the size of the damage reaches a size N_D, the filament is severed. On the other hand, if the size reaches zero, then the damage is repaired. Thus, the size of the damage x measured in subunits (i.e., tubulin dimers) is modeled as a one-dimensional random walk with absorbing boundaries at $x = 0$ and $x = N_D$.

The probability of severing $P_{sev}(x)$ is the probability that 1-D random walker, starting at position $x(0 \leq x \leq N_D)$ reaches the $x = N_D$ boundary before repair occurs, i.e., before $x = 0$ is reached. In this case, the probability of severing when the damage size is 0, i.e., $P_{sev}(x = 0) = 0$ and probability of severing when the damage size is N_D i.e., $P_{sev}(x = N_D) = 1$. These two conditions will serve as our two boundary conditions.

If $0 < x < N_D$, then, we can write the following recursion equation

$$P_{sev}(x) = (1 - P_{rm})P_{sev}(x - 1) + P_{rm}P_{sev}(x + 1) \qquad \text{(Equation 3)}$$

where $P_{rm} = k_r/(k_r + k_T[T])$ is the probability of damage spot increasing in size (subunits being removed from the site) and $1 - P_{rm}$ is the probability of damage spot decreasing in size (subunits being added at the site).

We use the method of characteristic equations to solve the recursion equation. Substituting, $P_{sev}(x - 1) = 1, P_{sev}(x) = s$ and $P_{sev}(x + 1) = s^2$, we get

$$P_{rm}s^2 - s + (1 - P_{rm}) = 0 \qquad \text{(Equation 4)}$$

whose two solutions are $s_{1,2} = 1, \frac{1-P_{rm}}{P_{rm}}$. Solutions to (1) are $P_{sev}(x) = A(s_1)^x + B(s_2)^x$. Substituting, we get $P_{sev}(x) = A\left(\frac{1-P_{rm}}{P_{rm}}\right)^x + B$. Using boundary conditions, $P_{sev}(0) = 0, P_{sev}(N_D) = 1$, we get $B = -A$ and $A = \frac{1}{\left(\frac{1-P_{rm}}{P_{rm}}\right)^{N_D} - 1}$. We define a dimensionless tubulin concentration

$\tilde{T} = \frac{1-P_{rm}}{P_{rm}} = \frac{k_T[T]}{k_r} = \frac{[T]}{[T]_c}$ which is the ratio of the tubulin concentration and a critical concentration $[T]_c$, which is the tubulin concentration where the rate of repair is equal to rate of severing, equal to k_r/k_T. We find that $P_{sev}(x,[T]) = \frac{\tilde{T}^x - 1}{\tilde{T}^{N_D} - 1}$, which is a function of Tubulin concentration. We note that when $\tilde{T} \ll 1$, $P_{sev}(x,[T]) \approx 1 - \tilde{T}^x$ and when $\tilde{T} \gg 1$, $P_{sev}(x,[T]) \approx \left(\frac{1}{\tilde{T}}\right)^{N_D - x}$. Also, $P_{sev}(x,[T]) \leq \frac{\tilde{T}^x}{\tilde{T}^{N_D}} = \left(\frac{k_r}{k_T[T]}\right)^{N_D - x}$, hence as the tubulin concentration increases, $P_{sev}(x)$ decreases (Figures 2 and S3).

If we assume an initial damage of size $x = 1$, as we do in the manuscript, then $P_{sev}(x = 1, [T]) = \frac{\tilde{T} - 1}{\tilde{T}^{N_D} - 1}$ which is approximately equal to $\left(\frac{1}{\tilde{T}}\right)^{N_D - 1}$ when $\tilde{T} \gg 1$ and $P_{sev}(x,[T]) \approx 1 - \tilde{T}$ when $\tilde{T} \ll 1$. In other words, above the critical tubulin concentration, the probability of severing becomes a very sensitive function (large power) of the tubulin concentration.

Calculation for time to either sever or repair

Let $T_{end}^*(x)$ be the average time (in steps) it takes to for the filament to either get severed or repaired, starting with a damage of size x. On the first step, the damage spot can either get replenished with subunits with a probability $1 - P_{rm}$ or increase in size by having subunits removed with a probability P_{rm} in time Δt i.e.,

$$T_{end}^*(x) = \Delta t + T_{end}^*(x - \Delta x)(1 - P_{rm}) + T_{end}^*(x + \Delta x)P_{rm}$$

There are two possible boundary conditions, $T_{end}^*(0) = T_{end}^*(N_D) = 0$. Using $\Delta x = \Delta t = 1$, we get a recursion relation similar to the one before, i.e., $T_{end}^*(x) = T_{end}^*(x - 1)(1 - P_{rm}) + T_{end}^*(x + 1)P_{rm} + 1$, which is an inhomogeneous recursion relation.

We first find the solution to the homogeneous equation:

$$T_{end}^*(x - 1)(1 - P_{rm}) - T_{end}^*(x) + T_{end}^*(x + 1)P_{rm} = 0$$

This is similar to the one we solved in "calculation of probability of severing" section. Following the same method, we can show that the solution is $T_{end}^{*homogenous}(x) = A\left(\frac{1-P_{rm}}{P_{rm}}\right)^x + B$ and the solution to inhomogeneous equation we have to guess (since the inhomogeneous is a constant) $T_{end}^{*inhomogenous}(x) = Cx + D$

Substituting it in the equation for $T_{end}^*(x)$ we get $C = \frac{1}{1 - 2P_{rm}}$ and the inhomogenous solution is valid for all values of D. The complete solution is $T_{end}^*(x) = T_{end}^{*homogenous}(x) + T_{end}^{*inhomogenous}(x)$ which is $T_{end}^*(x) = A\left(\frac{1-P_{rm}}{P_{rm}}\right)^x + B + \frac{x}{1 - 2P_{rm}}$

Using the boundary conditions, and assuming $P_{rm} \neq 1/2$, we find $T_{end}^*(x) = \frac{x}{1 - 2P_{rm}} - \frac{N_D}{1 - 2P_{rm}} \frac{\left(\frac{1-P_{rm}}{P_{rm}}\right)^x - 1}{\left(\frac{1-P_{rm}}{P_{rm}}\right)^{N_D} - 1}$. When $P_{rm} = 1/2$, $T_{end}^*(x) = x(N_D - x)$.

Note that $T_{end}^*(x)$ is the time (in steps) taken to reach either end (filament gets repaired or severed). We get time taken by a damage spot to be repaired or severed, i.e., $T_{end}(x)$ by multiplying time in steps by $\Delta t_{avg} = \frac{1}{k_T[T] + k_r}$,

$$T_{end}(x,[T]) = \left(\frac{1/k_r}{\tilde{T} + 1}\right)\left(\frac{\tilde{T} + 1}{\tilde{T} - 1}\right)\left(x - N_D\left(\frac{\tilde{T}^x - 1}{\tilde{T}^{N_D} - 1}\right)\right) \qquad \text{(Equation 5)}$$

where $P_{rm} = \frac{k_r}{k_r + k_T[T]}$ and $\tilde{T} = \frac{1-P_{rm}}{P_{rm}} = \frac{k_T[T]}{k_r}$. Equation 5 for $(x = 1)$ is plotted in Figure S3C.

Calculation of severing time

In this section, we derive an expression for time it takes to sever (Equation 1 in main text) a filament. In the one-dimensional random walk model for damage spreading, there are two ways to reach the end – either get severed or get repaired. Hence, the time to reach either end is given by the following equation,

$$T_{end}(x) = P_{sev}(x)T_{sev}(x) + (1 - P_{sev}(x))T_{sev}(N_D - x) \qquad \text{(Equation 6)}$$

where $T_{end}(x)$ is the time to reach either end if the initial size of the damage is x, $T_{sev}(x)$ is the time to sever and $P_{sev}(x)$ is the probability to sever when starting at x. Using the expression for $T_{end}(x)$ which we computed in section "Calculation for time to either sever or repair", we can extract $T_{sev}(x)$.

Replacing x with $N_D - x$ in Equation 6 we get, $T_{end}(N_D - x) = P_{sev}(N_D - x)T_{sev}(N_D - x) + (1 - P_{sev}(N_D - x))\, T_{sev}(x)$. Using $P_{sev}(x) = \frac{\tilde{T}^x - 1}{\tilde{T}^{N_D} - 1}$ and $P_{sev}(N_D - x) = \frac{\tilde{T}^{N_D - x} - 1}{\tilde{T}^{N_D} - 1}$, we get $1 - P_{sev}(x) = \frac{\tilde{T}^{N_D} - \tilde{T}^x}{(\tilde{T}^{N_D} - 1)} = \tilde{T}^x P_{sev}(N_D - x)$ and $1 - P_{sev}(N_D - x) = \frac{\tilde{T}^{N_D} - 1 - \tilde{T}^{N_D - x} + 1}{\tilde{T}^{N_D} - 1} = \frac{\tilde{T}^{N_D - x}(\tilde{T}^x - 1)}{\tilde{T}^{N_D} - 1} = \tilde{T}^{N_D - x} P_{sev}(x)$.

From the previous section, $T_{end}(x) = \left(\frac{1/k_r}{\tilde{T}+1}\right)\left(\frac{\tilde{T}+1}{\tilde{T}-1}\right)\left(x - N_D\left(\frac{\tilde{T}^x - 1}{\tilde{T}^{N_D} - 1}\right)\right) = \left(\frac{1}{k_T[T]+k_r}\right)\left(\frac{\tilde{T}+1}{\tilde{T}-1}\right)(x - N_D P_{sev}(x))$.

Substituting the expression for $1 - P_{sev}(x)$ and $1 - P_{sev}(N_D - x)$ in the equations for $T_{end}(x)$ and $T_{end}(N_D - x)$, we get

$$T_{sev}(x) = \frac{T_{end}(x) - \tilde{T}^x T_{end}(N_D - x)}{P_{sev}(x)\left(1 - \tilde{T}^{N_D}\right)} \qquad \text{(Equation 7)}$$

After substituting expression for $T_{end}(x)$ and $T_{end}(N_D - x)$ in Equation 5, we get

$$T_{sev}(x) = \left(\frac{1}{k_T[T]+k_r}\right)\left(\frac{\tilde{T}+1}{\tilde{T}-1}\right)\left(\frac{x - N_D P_{sev}(x) - \tilde{T}^x\left(N_D\left(\tilde{T}^{N_D - x} P_{sev}(x)\right) - x\right)}{P_{sev}(x)\left(1 - \tilde{T}^{N_D}\right)}\right).$$

Finally, after substituting the expression for $P_{sev}(x) = \frac{\tilde{T}^x - 1}{\tilde{T}^{N_D} - 1}$ and moving terms around, we get

$$T_{sev}(x) = \left(\frac{1/k_r}{\tilde{T}+1}\right)\left(\frac{\tilde{T}+1}{\tilde{T}-1}\right)\left(N_D\frac{(1+\tilde{T}^{N_D})}{(\tilde{T}^{N_D} - 1)} - \frac{x(\tilde{T}^x + 1)}{(\tilde{T}^x - 1)}\right) \qquad \text{(Equation 8)}$$

For an initial damage size $x = 1$, $T_{sev}(k_T, k_r, N_D) = \left(\frac{1/k_r}{\tilde{T}-1}\right)\left(N_D\frac{(\tilde{T}^{N_D}+1)}{(\tilde{T}^{N_D} - 1)} - \frac{\tilde{T}+1}{\tilde{T}-1}\right)$, which is the equation we used to plot the mean severing time in Figures 1D and S3C inset (see SI).

$T_{sev}(k_T, k_r, N_D)$ has two limits: (1) When $\tilde{T} \ll 1$, and $N_D \gg 1$, $T_{sev}(k_T, k_r, N_D) = -\left(\frac{1/k_r}{1-\tilde{T}}\right)\left(-N_D + \frac{\tilde{T}+1}{1-\tilde{T}}\right) \sim \frac{N_D}{k_r}\left(\frac{1}{1-\tilde{T}}\right) \sim \frac{N_D}{k_r}\left(1 + \tilde{T}\right)$; the severing time is linear in tubulin concentration. (2) When $\tilde{T} \gg 1$, and $N_D \gg 1$, $T_{sev}(k_T, k_r, N_D) = \left(\frac{1}{k_r\tilde{T}}\right)(N_D)$; the severing time decreases as tubulin concentration increases. These limiting behaviors imply that the severing time has a maximum as a function of tubulin concentration, which is obtained at a concentration that is of the order critical tubulin concentration $[T]_c = \frac{k_r}{k_T}$.

In diffusive limit, the rates of damage spreading and repair are balanced, i.e., $\tilde{T} = 1$ and $\lim_{\tilde{T} \to 1} P_{sev}(x, N_D) = x/N_D$. Let w_x be the probability of removing a monomer when the damage size is x, conditioned on successful completion of severing, then $w_x = \frac{P_{rm} P_{sev}(x+1)}{P_{rm} P_{sev}(x+1) + (1 - P_{rm})P_{sev}(x-1)}$. For $\tilde{T} = 1$, $w_x = \frac{(x+1)}{2x}$. Then the recurrence relation for $T^*_{sev}(x)$, the expected time of the severing (in steps) starting at x conditioned on completing severing is given by

$$T^*_{sev}(x) = 1 + w_x\left(T^*_{sev}(x + 1)\right) + (1 - w_x)\left(T^*_{sev}(x - 1)\right)$$

with the boundary conditions for $T^*_{sev}(N_D) = 0$ and $T^*_{sev}(2) - T^*_{sev}(1) = -1$. The homogeneous equation of the recurrence is identical to the one solved for $P_{sev}(x)$ and $T^*_{end}(x)$ and hence the solution is $T^{*homogenous}_{sev}(x) = A\left(\frac{1-w_x}{w_x}\right)^x + B$. For the inhomogenous equation, we try the solution $T^{*inhomogenous}_{sev}(x) = Cx^2$.

Substituting $T^{*inhomogenous}_{sev}(x) = Cx^2$, $T^{*inhomogenous}_{sev}(x - 1) = C(x - 1)^2$ and $T^{*inhomogenous}_{sev}(x + 1) = C(x+1)^2$ in the recurrence equation, we get $Cx^2 = 1 + w_x C(x+1)^2 + (1 - w_x)C(x - 1)^2$, which leads to $C = -\frac{1}{3}$.

The full solution is thus:

$$T^*_{sev}(x) = \left(\frac{1 - w_x}{w_x}\right)^x + B - \frac{x^2}{3} = A\left(\frac{x - 1}{x+1}\right)^x + B - \frac{x^2}{3}$$

Using the boundary conditions, we can find $A = 0$, and $B = \frac{N^2}{3}$, which results to $T^*_{sev}(x, N) = \frac{1}{3}(N^2 - x^2)$. Since $T^*_{sev}(x)$ is the time (in steps), we get time taken by a damage spot to be severed, i.e., $T_{sev}(x)$ by multiplying time in steps by $\Delta t_{avg} = \frac{1}{k_T[T]+k_r} = \frac{1}{2k_r}$. Hence, at $\tilde{T} = 1$, $T_{sev}(x) = \frac{1}{6k_r}(N^2 - x^2)$. Alternatively, we can take the limit of $\tilde{T} \to 1$ in the Equation 8, i.e., $\lim_{\tilde{T} \to 1} T_{sev}(k_T, k_r, x, N_D)$ to get the same result.

Calculation of probability distribution of filament lengths, due to severing with and without repair

In ref.,[54] we considered the case of a uniform rate of severing along a filament; in other words, severing takes place anywhere along the filament with equal probability. A filament consisting of ℓ subunits can be broken into two smaller filaments at any of the $(l - 1)$ positions with an equal rate s, for any choice of severing location; the total rate of severing at any location is then, $s(l - 1)$. In addition to the severing rate, there is r, the rate at which subunits are added to a filament. Using these two rates we find an expression for the probability distribution of lengths at steady state (reproduced from ref.[54]), $P(l) = \frac{l\, s\, r^{l-1}}{(r+s)(r+2s)(r+3s)\dots(r+ls)}$, which can be further simplified to

$$P(l) \;=\; \frac{l\,s\,r^{l-1}}{r^l\left(1+\frac{s}{r}\right)\left(1+\frac{2s}{r}\right)\cdots\left(1+\frac{ls}{r}\right)} \;=\; \frac{ls}{r}e^{-\frac{s}{r}\sum_{j=1}^{l}j} \;=\; \frac{ls}{r}e^{-\frac{s}{r}\frac{l(l+1)}{2}} \qquad \text{(Equation 9)}$$

Here we use the approximation that $e^{js/r} = 1 + \frac{js}{r}$ which is valid for $js \ll r$. For $l \gg 1$, $P(l) = \frac{ls}{r}e^{-\frac{s}{r}\frac{l^2}{2}}$ and we use this expression to plot the distribution of lengths without repair with rates $r = k[T]$ and $s = k_d[S]$, and with repair with the rates $r = k[T]$ and $s = k_d[S]P_{sev}([T])$ in Figure 3D.

Additionally, we can use this approximation to compute the mean $<l>$ and variance of the filament length distribution, $<l^2> - <l>^2$. In

general, moments are defined as, $<l^n> = \frac{\int l^n P(l)dl}{\int P(l)dl}$. For the mean, $n = 1$, and hence $<l> = \dfrac{\int l^2 \frac{s}{r}e^{-\frac{s}{r}\frac{l^2}{2}}dl}{\int \frac{ls}{r}e^{-\frac{s}{r}\frac{l^2}{2}}dl}$.

Using the properties of Gaussian integrals, $\displaystyle\int_0^\infty e^{-\alpha\frac{l^2}{2}}dl = \frac{1}{2}\sqrt{\frac{2\pi}{\alpha}}$, we can show $\displaystyle\int_0^\infty le^{-\alpha\frac{l^2}{2}}dl = \frac{1}{\alpha}$, and $\displaystyle\int_0^\infty l^3 e^{-\alpha\frac{l^2}{2}}dl = \frac{2}{\alpha^2}$. Substituting these

results, we get $<l> = \dfrac{\int \alpha l^2 e^{-\alpha\frac{l^2}{2}}dl}{\int \alpha l e^{-\alpha\frac{l^2}{2}}dl} = \sqrt{\frac{\pi}{2\alpha}}$ and $<l^2> = \dfrac{\int l^3 e^{-\alpha\frac{l^2}{2}}dl}{\int l e^{-\alpha\frac{l^2}{2}}dl} = \frac{2}{\alpha}$.

The variance, $<l^2> - <l>^2$, is $\frac{2}{\alpha} - \frac{\pi}{2\alpha}$ and standard deviation, $\sigma = \sqrt{\frac{1}{\alpha}\left(2 - \frac{\pi}{2}\right)}$. We define "Noise" or the coefficient of variation as $\frac{\sigma}{<l>} = \sqrt{\frac{2-\frac{\pi}{2}}{\frac{\pi}{2}}} = \sqrt{\frac{4}{\pi} - 1} = 0.523$, which is a prediction for the uniform severing mechanism. We use this relationship to plot Figure 3D, inset.

Additionally, substituting $\alpha = \frac{k_d[S]}{k[T]}$ in to the expression for the mean and variance of filament lengths at steady state, we get, $L_s^{simple\ severing} = <l> = \sqrt{\frac{\pi k[T]}{2\,k_d[S]}}$, and substituting $\alpha = \frac{k_d[S]P_{sev}([T])}{k[T]}$, we find $L_s^{with\ repair} = \sqrt{\frac{\pi k[T]}{2\,k_d[S]P_{sev}([T])}}$, which is used in Figure 3C.

Note that $L_s^{with\ repair}$ has two regimes: When $[T] < [T]_c$, $P_{sev}([T]) \approx 1 - \tilde{T}$, $L_s \sim \sqrt{[T]}$. When $[T] > [T]_c$, $P_{sev}([T]) \approx \left(\frac{1}{\tilde{T}}\right)^{N_D-1}$ and, $L_s \approx [T]^{N_D/2}$.

QUANTIFICATION AND STATISTICAL ANALYSIS

Estimation of parameters

In this section, we compare our theoretical predictions with experimental data from ref. [20] (obtained directly from Roll-Mecak lab), and extract values for the parameters of our model. In particular we focus on Figures 3D and 3H in ref.,[20] where the authors plot probability to sever and time taken to sever for different concentrations of tubulin.

Our model for severing with repair has four parameters - k_T, k_r, x and N_D. In Equation 8, we find an expression for the mean severing time as a function of the tubulin concentration. We assume an initial damage of size $x = 1$, and constrain the space of possible parameter values using experimental data in ref.[20] In Equation 4, we predict that the probability of severing decreases as N_D increases (Figure S3). We use the observation of severing events at $[T] = 5\ \mu M$ in ref. [20] to constrain N_D (upper bound = 40) by assuming that probability of severing is at least 10^{-3}. We obtain a rough lower bound for $N_D \approx 20$ from the TEM images in Figure 1 in ref. [20] showing patches of tubulin removed from microtubules which are still intact. Next, we use the method of least squares on this constrained parameter range to find sets of parameters that fit the published data Figure 3H in ref. [20] which reports the mean and the standard deviation of severing times as a function of tubulin concentration (Figure S1). Our estimated values are: $k_T = 0.11\ \mu M^{-1}s^{-1}$, $k_r = 0.54\ s^{-1}$ and $N_D = 25$. Using these estimated values, we plot the severing time and the probability of severing in Figures 2A and 2B respectively.

Sensitivity analysis of parameters

As seen in Figure S1, probability of severing increases with a larger initial damage size x but severing time is unaffected. Probability of severing is unaffected by N_D but time to sever increases with a larger N_D. As is captured by the analytical formula in Equation 2 in main text, the critical concentration of tubulin $[T_c]$ where the time of severing starts decreasing, is unaffected by x and N_D.

Comparison of experiment and theory via bootstrapping

In Figure 1 in the main text, we show a comparison of experimental data from[20] with a theoretical curve for mean severing time and simulation curve for standard deviation of severing time using our fitted parameters. Since ref. [20] reported mean severing time and standard deviation of severing time, we used a bootstrapping scheme using data resampling to compute the error on the mean (error bars in Figure 1C), and error on the standard deviation (error bars in Figure 1D(inset)). The error bars on the mean severing time and standard deviation of severing times were calculated from 750 bootstrapping samples.

Stochastic simulation schemes

Model for severing with repair

A severing event begins when a severing protein lands on a filament, binds to the side, and creates a damage of size x. The fate (eventual severing or repair) of the damage created by a severing protein is determined by a competition between the removal and addition of tubulin at the damage site. We use the Gillespie algorithm to simulate this process - subunits are added to the damage site at a rate proportional to the concentration of free tubulin $k_T[T]$ (s^{-1}) and are removed from the damage site at a rate k_r (s^{-1}), with each step either increasing or decreasing the size of damage. If the size of the damage reaches a size N_D, the filament is severed. On the other hand, if the size reaches zero, then the damage is repaired. By performing this simulation multiple times (typically about 13,000 severing events), we obtain, as a function of tubulin concentration, the probability of severing (Figure 2), the mean severing time (Figure 1C) and the probability distribution of severing times (Figure 1D).

Length trajectory with repair-severing

Simulation of filament growth is performed using a Gillespie algorithm. At each step of the simulation, either the filament gains one subunit, with probability proportional to the concentration of tubulin ($k[T]$), or it gains a new severing site when a severing protein lands on the filament at position between 1 and $l-1$, with probability k_r, where ℓ is the length of the filament. In the absence of competition between severing and repair, a severing event occurs immediately upon creating. However, if competition is considered, each time a severing site is created, a severing event occurs at this site with a probability $P_{sev}(x)$ in Equation 3.

Filament growth with finite severing time

In order to incorporate a finite severing time into our simulation, we first run our damage spreading simulation (A) to create a distribution of severing times. Then, we adjust the filament growth simulation in (B) by tracking the location of each damage site (where severing protein binds) on our microtubule. The severing occurs with a probability given by Equation 4. For every severing event, we assign a severing time by sampling it from our distribution of severing times. Once this time has surpassed in the simulation, the microtubule is severed at this damage site. We keep track of one part of the severed microtubule. The other part, and any damage sites on that part, are removed.

Conversion between monomer number and filament length

Microtubules are hollow cylinders and made up of 13 protofilaments built up from tubulin dimers, each 4 nm in length. A cross section of a microtubule is a ring of 13 dimers that is 4 nm wide. Our simulations are based in subunits. We use the following conversion to convert from subunits to length: 1 subunit = 4/13 nm.

Effect of finite severing time on microtubule dynamics

If the severing protein binding time is comparable to severing time, it is possible that, after one severing event, there are other damage sites on the filament which will lead to a severing event shortly thereafter. This will produce correlations in subsequent severing events which we ignore when deriving our analytic formulas for P_{sev} and T_{sev}. In order to account for this situation, we performed a simulation where we allowed multiple damage sites on a microtubule lattice at one time. We observed that our results of large dynamic range in steady-state length from the full simulation are similar to what was seen with the simple model where we assumed a negligible severing time (Figure S5). The coefficient of variation (CV) of filament lengths at steady state calculated in the full simulation was identical to the one obtained from the simple model at low and high tubulin concentration. However, at intermediate values of tubulin concentrations, we observed a peak in the CV as seen in Figure S5C, which was in contrast to the constant value seen with the simple model (Figure 3D). We observed that the peak in CV depends on the concentration of severing protein as shown in Figure S5D. As shown in inset, the variation from the typical constant value occurs when the time between binding events which can lead to severing (computed by $\frac{1}{k_d[S]} \frac{1}{L_s} \frac{1}{P_{sev}}$ where L_s is the length of microtubule) is less than the time it takes to sever.

Effect of dynamic instability and severing on microtubule dynamics

The simulation that includes dynamic instability follows the same algorithm as that detailed earlier in STAR methods, with inclusion of an additional boolean parameter for whether the microtubule is in a state of rescue or catastrophe. In the rescue state, the microtubule grows (gain subunits) at a rate proportional to the tubulin concentration, $c_T[T]$. During catastrophe, the microtubule loses subunits at a rate c_s. The microtubule can undergo severing in either state. At each timestep, the microtubule can a) grow or shrink depending on whether it is in catastrophe or rescue, b) have a severing protein land and either sever the filament or not depending on the outcome of the competition between severing and repair, or c) switch from catastrophe to rescue or rescue to catastrophe. We use the parameters[70,85] listed in Tables 1 and S1 for our stochastic simulations. As before, we find that the dynamic range of the mean length of microtubules is greater when the repair process is included (Figure S6). However, coefficient of variation shows a non-monotonic relationship with tubulin concentration.